Communication

Hierarchically Ordered 2-Dimensional Coordination Polymers Assembled from Redox-Active Dimolybdenum Clusters

F. James Claire, Stephanie M. Tenney, Minyuan M. Li, Maxime A. Siegler, Justine S. Wagner, Anthony Shoji Hall, and Thomas J Kempa

J. Am. Chem. Soc., **Just Accepted Manuscript** • DOI: 10.1021/jacs.8b06331 • Publication Date (Web): 15 Aug 2018

Hierarchically Ordered 2-Dimensional Coordination Polymers Assembled from Redox-Active Dimolybdenum Clusters

F. James Claire,[†,^] Stephanie M. Tenney,[†,^] Minyuan M. Li,[†,^] Maxime A. Siegler,[†] Justine S. Wagner,[‡] Anthony S. Hall,[‡] Thomas J. Kempa*[,†,‡]

[†] Department of Chemistry, The Johns Hopkins University, Baltimore, Maryland 21218, USA

[‡] Department of Materials Science and Engineering, The Johns Hopkins University, Baltimore, Maryland 21218, USA

Supporting Information Placeholder

ABSTRACT: Coordination polymers (CPs) supporting tunable through-framework conduction and responsive properties are of significant interest for enabling a new generation of active devices. However, such architectures are rare. We report a redox-active CP comprised of two-dimensional (2D) lattices of coordinatively bonded $Mo_2(INA)_4$ clusters (INA=isonicotinate). The 2D lattices are commensurately stacked and their ordering topology can be synthetically tuned. The material has a hierarchical pore structure (pore sizes distributed between 7–33 Å) and exhibits unique CO_2 adsorption (nominally Type VI) for an isotherm collected at 195 K. Furthermore, cyclic voltammetry and electrokinetic analyses identify a quasi-reversible feature at $E_{1/2}$ = –1.275 V versus ferrocene/ferrocenium that can be ascribed to the $[Mo_2(INA)_4]^{0/-1}$ redox couple, with an associated standard heterogeneous electron transfer rate constant k_s = 1.49 s^{-1}. The tunable structure, porosity, and redox activity of our material may render it a promising platform for CPs with responsive properties.

Coordination polymers (CPs) are characterized by a diversity of architectures, porosities, and chemistries that collectively render them useful in gas and ion occlusion, separations, and catalysis.[1–9] Recently, significant interest has focused on the development of responsive CPs that could enable a new generation of *active* device architectures including filters, switches, membranes, and sensors.[9,10] The incorporation of redox tunable states in CPs and covalent organic frameworks (COFs) is one approach to engender a responsive framework with functional properties of scientific and technological importance.[11] The post-synthetic incorporation of redox-active species into the pores of metal-organic frameworks (MOFs) has yielded impressive architectures exhibiting conductivity, enhanced structural stability, and even catalytic activity.[12] However, despite recent progress in design of conductive frameworks,[1,2,13] development of CPs exhibiting through-framework conduction *via* the redox-states of their constituent metal or ligand centers has received less attention.

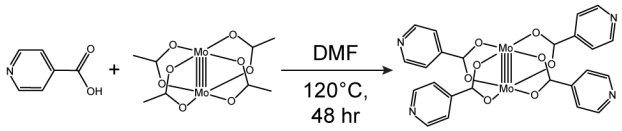

Figure 1. Ligand exchange reaction yielding $Mo_2(INA)_4$.

We identified $Mo_2(INA)_4$ as the molecular building block for our candidate responsive CP material. This cluster is composed of a quadruply-bonded dimolybdenum core $(Mo_2)^{4+}$ coordinated by 4 equatorial isonicotinate (INA) ligands and exhibits several features of interest. First, the two strongly coupled Mo atoms can support a delocalized Class III Robin-Day[14] mixed-valence state. This mixed-valence Mo_2 core, if coupled effectively to neighboring ligands, could support long-range through-framework charge transfer. Second, the potential to tune the redox state of this di-Mo core could render a desired responsive material. Third, the heterotopic equatorial INA ligands, and open axial coordination sites on the Mo_2 core, provide synthetic versatility for assembly of various crystal topologies.

Our efforts take inspiration from the literature on preparation and exploration of di-nuclear transition metal clusters. Previous efforts have focused on the synthesis, theoretical treatment, and electronic spectroscopy of the di-atomic clusters, ions, and metal-ligand clusters of the 1st and 2nd row transition metals.[15–17] Within this context, research has focused on molecular complexes[18] and cages[19] containing Mo_2 cores, and on supramolecular arrays of isolated M_2 (M=Mo, Rh, Ru) dimers and polyhedra.[20] However, to the best of our knowledge, examples of CPs composed of quadruply bonded di-nuclear 2nd row transition metal clusters are rare.[21]

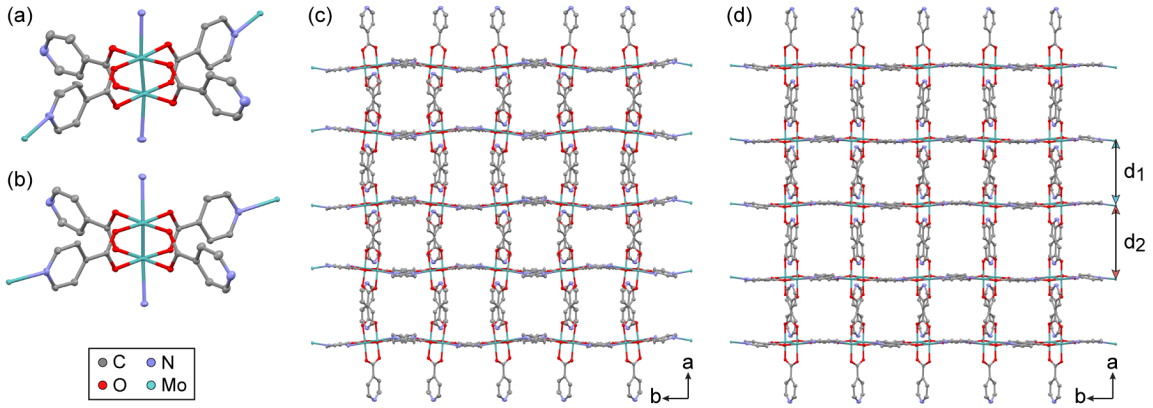

Figure 2. (a) Crystal structure of the $Mo_2(INA)_4$ cluster used to assemble **I**. (b) Crystal structure of the $Mo_2(INA)_4$ cluster used to assemble **II**. (c) Crystal packing structure of **I** viewed down the *c* axis. (d) Crystal packing structure of **II** viewed down the *c* axis. Hydrogen atoms and lattice solvent molecules omitted for clarity. Displacement ellipsoids given at 50 % probability.

We also note that despite reports, which harken back to the early 20th century, discussing the importance of mixed-valence complexes such as Prussian blue,[14] to-date, demonstrations of coordination polymers exhibiting mixed-valence mechanisms are still rare.[1,2,13,22–26]

We prepared the aforementioned $Mo_2(INA)_4$ cluster through a ligand exchange reaction (Figure 1). Reaction of dimolybdenum tetraacetate with 10 equivalents of isonicotinic acid at 120 ˚C in dimethylformamide yields a bright red powder. Mass spectrometry of this powder identified a feature at 680 *m*/*z* (Figure S1). This ratio corresponds to the molar mass of $Mo_2(INA)_4$, the desired molecular building block.

To assemble CPs from this cluster, we performed recrystallizations from solutions containing $Mo_2(INA)_4$ and either only dimethylacetamide (DMA) or DMA and 1,4-diazabicyclo[2.2.2]octane (DABCO). Recrystallization at room temperature over the course of 2 days yielded dark red single crystals from DMA solutions (**I**) and from DMA and DABCO solutions (**II**). Crystal structures obtained through single-crystal X-ray diffraction (XRD) experiments (Figure S2) conducted at 110 K on **I** (Figure 2a, c) and on **II** (Figure 2b, d) identify several salient features of the new CP frameworks. First, both paddlewheel nodes of the framework (Figure 2a, b) consist of 2 bonded Mo atoms coordinated to the carboxylate groups of 4 INA ligands. Second, the Mo–Mo bond distances in **I** and **II** are 2.1211(4) Å and 2.1227(3) Å, respectively. These distances are within 2 % of the Mo–Mo bond distances observed in quadruply bonded Mo_2 cores coordinated by 3-atom bridging ligands.[27] Third, each Mo is bonded to the pyridyl-N of the INA ligand of an adjacent node with Mo–N bond distances within **I** and **II** ranging between 2.546(3) Å and 2.586(3) Å. These coordination bonds give rise to a 2D lattice of $Mo_2(INA)_4$ nodes (Figure S3). Finally, packing diagrams viewed down the *c* axis of both **I** and **II** (Figure 2c, d) show that the crystals (space groups, **I**: $P2/c$ and **II**: $P2_1/c$) are porous and composed of the 2D lattices stacked commensurately atop one another. Together, these data show successful assembly of CPs composed of $Mo_2(INA)_4$ clusters joined into a 2D lattice.[28,29]

A detailed analysis of the structures of **I** and **II** identifies several features of our 2D material that are sensitive to recrystallization condition. The 2D (100) lattice planes of **I** and **II** are comprised of slightly distorted square sub-cells containing 4 coordinatively-bonded $Mo_2(INA)_4$ nodes (Figure S3). The in-plane diagonals of these sub-cells are 14.015 Å and 12.991 Å, and 14.313 Å and 12.809 Å for **I** and **II**, respectively. Furthermore, while the (100) lattice planes in **I** are separated by an average interplanar spacing of 8.190 Å, those in **II** regularly alternate between two distinct *d* spacings: d_1 = 7.854 Å and d_2 = 8.565 Å (Figure 2c, d). In the structure of **I**, the lattice DMA solvent molecules show significant disorder in their packing orientation and pore occupancy (Figure S4a). In the structure of **II**, the lattice DMA orients parallel (perpendicular) to the (100) lattice planes in the interplanar space having a thickness d_1 (d_2) (Figure S4b). Previously, DABCO has been integrated into MOFs as a pillaring ligand intended to organize square-grid layered structures into 3D open frameworks.[30] Notably, crystal structures and acid digestions of bulk crystalline samples of **II** verify that no DABCO is present in **II** (Figure S5). In summary, though DABCO does not integrate into **II**, it does appear to facilitate improved crystalline ordering and the alternate interplanar spacing between 2D lattices. We hypothesize that DABCO plays a structure-directing role by reversibly binding to Lewis acidic coordination sites with an attendant modulation of crystal packing.

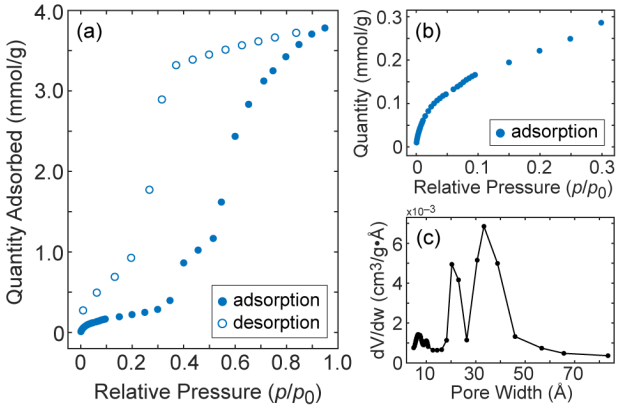

Figure 3. (a) Adsorption and desorption portions of the CO_2 isotherm collected at 195 K on **I**. (b) Expanded view of the CO_2 adsorption isotherm in the 0–0.3 p/p_0 region. (c) Differential pore volume (dV/dw) data identifying pore sizes in **I**.

Having established the long-range crystalline order of 2D CPs prepared from $Mo_2(INA)_4$ precursor, we set out to assess their porous characteristics through Brunauer-Emmett-Teller (BET) analysis. BET analysis of CO_2 adsorption and desorption for isotherms collected at 195 K on **I** reveals several unique features (Figure 3a, b). Adsorption data exhibit three distinct regions (*A*: 0–0.3 p/p_0; *B*: 0.3–0.5 p/p_0; *C*: 0.5–0.9 p/p_0) and can be broadly classified as belonging to a Type VI isotherm.[31] Only two distinct transitions are observed within the desorption data, and there is a significant hysteresis loop between adsorption and desorption data. Notably, N_2 adsorption and desorption data collected on **I** are characteristic of a Type III isotherm (Figure S6), which is associated with weak adsorbate-adsorbent interactions.[32] These data emphasize that **I** undergoes a unique interaction with CO_2, as compared to N_2. Furthermore, though the step-wise profile of the CO_2 isotherm suggests layer-by-layer filling of a range of pores *via* capillary condensation, we cannot rule out that strong interaction of CO_2 with **I** may induce structural transformation of the framework and result in increased CO_2 uptake at higher relative pressures.[32] We note that calculation of pore surface areas for complex isotherms that exhibit a number of distinct features is not trivial. Nevertheless, specific BET and Langmuir pore surface areas calculated from the adsorption isotherm within the 0.05–0.3 p/p_0 region (Figure 3b) and at saturation (0.95 p/p_0)[33] are 18.6 m^2/g and 505.1 m^2/g, respectively (Figure S7). Notably, pXRD data of **I** taken after BET analysis show that the crystal structure of **I** is well retained (Figure S8).

A plot of differential pore volume as a function of pore width was obtained through analysis of adsorption data with the Horvath-Kawazoe model (Figure 3c). The pore distribution data identify two narrow peaks associated with pore widths of 7 Å and 10 Å, and two broad peaks associated with pore widths of 20 Å and 33 Å. The former 2 peaks can be associated with CO_2 uptake by the ~13–14 Å pores formed by the square sub-cells comprising the 2D planes of **I** (Figure S3), while the latter 2 peaks may be associated with CO_2 uptake by pores in the interplanar space between 2D lattices. Integration of the differential pore width data shows that 84 % of the total adsorbed CO_2 is sequestered by pores > 20 Å in width. The unique CO_2 uptake properties of **I** are potentially a consequence of its hierarchical structure. In particular, it is possible that the crystal expands about the interplanar space to accommodate more CO_2 storage at higher relative pressures.[32–37] We note that the gas uptake properties reported herein are distinct from those reported in other layered 2D CPs[35,36] and 3D CPs.[21,38]

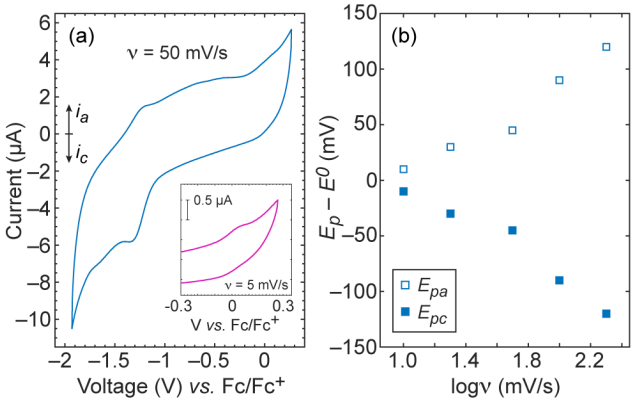

Figure 4. (a) CV of **I** in acetonitrile, TBA PF_6, and BMIM BF_4 collected at a scan rate of 50 mV/s. Inset: Expanded view of anodic wave in CV of **I** at ν = 5 mV/s. (b) Trumpet plot assembled from data of cathodic (E_{pc}) and anodic (E_{pa}) peak potentials as a function of scan rate (Figure S9).

Finally, we set out to assess whether our CPs have readily accessible redox states, which could mediate through-framework charge transfer and enable the use of these materials in future electronic devices. To this end, the redox properties of **I** were assessed through cyclic voltammetry (CV) and electrokinetic analysis of CV data taken at multiple scan rates. CV data of **I** taken at a scan rate (ν) of 50 mV/s in acetonitrile, 0.1 M tetrabutylammonium hexafluorophosphate (TBA PF_6) and 20 mM 1-butyl-3-methylimidazolium tetrafluoroborate (BMIM BF_4) identify several features (Figure 4a). First, a small anodic wave is apparent between –100 mV and +100 mV *vs.* the Fc/Fc^+ redox couple (Figure 4a, inset). Previously reported CV data of molecular dimers of quadruply bonded di-Mo clusters have identified oxidation waves at –90 mV[39] and +100 mV[40] relative to Fc/Fc^+ that were attributed to $[(^tBuCO_2)_3Mo_2]_2(\mu\text{-}O_2C\text{–}C_{10}H_6\text{–}CO_2)^{0/+1}$ and $[(^tBuCO_2)_3Mo_2]_2(\mu\text{-}O_2C\text{–}C_6F_4\text{–}CO_2)^{0/+1}$ couples, respectively. Therefore, we associate the modest anodic peak between –100 and +100 mV in CVs of **I** with the $[Mo_2(INA)_4]^{0/+1}$ couple.

Second, a quasi-reversible (i_{pa}/i_{pc} = 0.26) redox wave with $E_{1/2}$ = –1.275 V is apparent, and multiple CV scans taken at ν = 50 mV/s show retention of this redox wave (Figure S9). The cathodic and anodic peak potentials

associated with this feature are E_{pc} = –1.32 V and E_{pa} = –1.23 V, respectively, and their separation implies a 1 electron process. We note that reduction of a range of isonicotinates was previously reported[41] to occur at –2.2 V versus Ag/Ag^+ (~ –2.6 V vs. Fc/Fc^+), which is well outside of our scanned potential range. We consequently rule out the possibility that cathodic features in our reported CVs of **I** are due to reduction of INA ligand. Therefore, we assign the cathodic peak at –1.32 V to 1 electron reduction and associate the redox wave at $E_{1/2}$ = –1.275 V with the $[Mo_2(INA)_4]^{0/-1}$ couple. A subsequent electrokinetic analysis was used to determine the rate of electron transfer associated with this couple. CVs of **I** were collected at scan rates between 5 and 200 mV/s (Figure S10). These data show an increase, as a function of increasing scan rate, in the splitting of the cathodic and anodic peak potentials associated with this couple. This observation is consistent with the onset of electrochemical irreversibility as the electrode reaction becomes dominated by the kinetics of electron transfer at the electrode. Using these data, a plot of the difference between the cathodic or anodic peak potential and the mid-point potential for the couple versus the logarithm of the scan rate was prepared (Figure 4b). A Laviron analysis[42] of these data furnishes an apparent heterogeneous electron transfer (ET) rate constant k_s = 1.49 s^{-1} for the $[Mo_2(INA)_4]^{0/-1}$ couple, assuming a 1 electron process and a transfer coefficient $\alpha = 0.5$ (Figure S11).

In conclusion, we have demonstrated a redox-active and porous CP composed of 2D lattices assembled from $Mo_2(INA)_4$ clusters.

ASSOCIATED CONTENT

Supporting Information. *Contents*: Methods and Supporting Figures S1–S13 (PDF), and cif files for **I** and **II**. These materials are available free of charge at http://pubs.acs.org.

AUTHOR INFORMATION

Corresponding Author

* Thomas J. Kempa (tkempa@jhu.edu). **ORCID:** 0000-0002-1672-8325

Author Contributions

^ These authors contributed equally to this work.

ACKNOWLEDGMENT

T. J. K. and M. M. L. acknowledge funding from the Camille and Henry Dreyfus Foundation through the Postdoctoral Program in Environmental Chemistry. T. J. K. is grateful to Eric D. Bloch and Gregory Lorzing (U. Delaware) for helpful discussions and assistance with BET analysis. The authors acknowledge use of powder XRD facilities at the JHU Institute for Quantum Matter.

REFERENCES

1. Ziebel, M. E.; Darago, L. E.; Long, J. R. *J. Am. Chem. Soc.* **2018**, *140*, 3040.
2. Xie, L. S.; Sun, L.; Wan, R.; Park, S. S.; DeGayner, J. A.; Hendon, C. H.; Dinca, M. *J. Am. Chem. Soc.* **2018**, *140*, 7411.
3. Sumida, K.; Rogow, D. L.; Mason, J. A.; McDonald, T. M.; Bloch, E. D.; Herm, Z. R.; Bae, T.-H.; Long, J. R. *Chem. Rev.* **2012**, *112*, 724.
4. Hendon, C. H.; Rieth, A. J.; Korzynski, M. D.; Dinca, M. *ACS Cent. Sci.* **2017**, *3*, 554.
5. Bisbey, R. P.; Dichtel, W. R. *ACS Cent. Sci.* **2017**, *3*, 533.
6. Zhou, H.-C.; Kitagawa, S. *Chem. Soc. Rev.* **2014**, *43*, 5415.
7. Diercks, C. S.; Yaghi, O. M. *Science* **2017**, *355*, 923:1.
8. Garibay, S. J.; Wang, Z.; Tanabe, K. K.; Cohen, S. M. *Inorg. Chem.* **2009**, *48*, 7341.
9. Stavila, V.; Talin, A. A.; Allendorf, M. D. *Chem. Soc. Rev.* **2014**, *43*, 5994.
10. Sato, O. *Nat. Chem.* **2016**, *8*, 644.
11. D'Alessandro, *Chem. Comm.* **2016**, *52*, 8957.
12. Ullman, A. M.; Brown, J. W.; Foster, M. E.; Léonard, F.; Leong, K.; Stavila, V.; Allendorf, M. D. *Inorg. Chem.* **2016**, *55*, 7233.
13. Park, J. G.; Aubrey, M. L.; Oktawiec, J.; Chakarawet, K.; Darago, L. E.; Grandjean, F.; Long, G. J.; Long, J. R. *J. Am. Chem. Soc.* **2018**, *140*, 8526.
14. Robinson, M. B.; Day, P. *Adv. Inorg. Chem. Radiochem.* **1968**, *10*, 247.
15. Cotton, F. A.; Wiesinger, K. J. *Inorg. Chem.* **1991**, *30*, 871.
16. Norman, J. G.; Kolari, H. J.; Gray, H. B.; Trogler, W. C. *Inorg. Chem.* **1977**, *16*, 987.
17. Klotzbuecher, W.; Ozin, G. A. *Inorg. Chem.* **1977**, *16*, 984.
18. Cotton, F. A.; Liu, C. Y.; Murillo, C. A. *Inorg. Chem.* **2004**, *43*, 2267.
19. Ke, Y.; Collins, D. J.; Zhou, H.-C. *Inorg. Chem.* **2005**, *44*, 4154.
20. Cotton, F. A.; Lin, C.; Murillo, C. A. *Acc. Chem. Res.* **2001**, *34*, 759.
21. Kramer, M.; Schwarz, U.; Kaskel, S. *J. Mater. Chem.* **2006**, *16*, 2245.
22. Férey, G.; Millange, F.; Morcrette, M.; Serre, C.; Doublet, M. L.; Greneche, J. M.; Tarascon, J. M. *Angew. Chem. Int. Ed.* **2007**, *46*, 3259.
23. Takaishi, S.; Hosoda, M.; Kajiwara, T.; Miyasaka, H.; Yamashita, M.; Nakanishi, Y.; Kitagawa, Y.; Yamaguchi, K.; Kobayashi, A.; Kitagawa, H. *Inorg. Chem.* **2009**, *48*, 9048.
24. Kobayashi, Y.; Jacobs, B.; Allendorf, M. D.; Long, J. R. *Chem. Mater.* **2010**, *22*, 4120.
25. Otsubo, K.; Wakabayashi, Y.; Ohara, J.; Yamamoto, S.; Matsuzaki, H.; Okamoto, H.; Nitta, K.; Uruga, T.; Kitagawa, H. *Nat. Mater.* **2011**, *10*, 291.
26. Sheberla, D.; Sun, L.; Blood-Forsythe, M. A.; Er, S.; Wade, C. R.; Brozek, C. K.; Aspuru-Guzik, A.; Dinca, M. *J. Am. Chem. Soc.* **2014**, *136*, 8859.
27. Cotton, F. A.; Mester, Z. C.; Webb, T. R. *Acta. Crystallogr. Sect. B* **1974**, *B30*, 2768.
28. Wasielewski, M. R.; Wu, Y.-L.; Bobbitt, N. S.; Logsdon, J.; Powers-Riggs, N.; Nelson, J.; Liu, X.; Wang, T.; Snurr, R.; Hupp, J.; Farha, O.; Hersam, M. *Angew. Chem. Int. Ed.* **2018**, *57*, 3985.
29. Schneemann, A.; Vervoorts, P.; Hante, I.; Tu, M.; Wannapaiboon, S.; Sternemann, C.; Paulus, M.; Wieland, D. C. F.; Henke, S.; Fischer, R. A. *Chem. Mater.* **2018**, *30*, 1667.
30. Dybtsev, D. N.; Chun, H.; Kim, K. *Angew. Chem. Int. Ed.* **2004**, *43*, 5033.
31. Sing, K. S. W. *Pure Appl. Chem.* **1985**, *57*, 603.
32. Fletcher, A. J.; Thomas, M.; Rosseinsky, M. J. *J. Solid State Chem.* **2005**, *178*, 2491.
33. Taylor, M. K.; Runcevski, T.; Oktawiec, J.; Gonzalez, M. I.; Siegelman, R. L.; Mason, J. A.; Ye, J.; Brown, C. M.; Long, J. F. *J. Am. Chem. Soc.* **2016**, *138*, 15019.
34. Alhamami, M.; Doan, H.; Cheng, C.-H. *Materials*, **2014**, *7*, 3198
35. Kondo, A.; Noguchi, H.; Ohnishi, S.; Kajiro, H.; Tohdoh, A.; Hattori, Y.; Xu, W.-C.; Tanaka, H.; Kanoh, H.; Kaneko, K. *Nano Lett.* **2006**, *6*, 2581.
36. Ichikawa, M.; Kondo, A.; Noguchi, H.; Kojima, N.; Ohba, T.; Kajiro, H.; Hattori, Y.; Kanoh, H. *Langmuir* **2016**, *32*, 9722.

37. Kondo, A.; Kojima, N.; Kajiro, H.; Noguchi, H.; Hattori, Y.; Okino, F.; Maeda, K.; Ohba, T.; Kaneko, K.; Kanoh, H. *J. Phys. Chem. C* **2012**, *116*, 4157.
38. Wade, C. R.; Dinca, M. *Dalton Trans.* **2012**, *41*, 7931.
39. Barybin, M. V.; Chisholm, M. H.; Dalal, N. S.; Holovics, T. H.; Patmore, N. J.; Robinson, R. E.; Zipse, D. J. *J. Am. Chem. Soc*. **2005**, *127*, 15182.
40. Chisholm, M. H.; Feil, F.; Hadad, C. M.; Patmore, N. J. *J. Am. Chem. Soc.* **2005**, *127*, 18150.
41. Sevov, C. S.; Brooner, R. E. M.; Chénard, E.; Assary, R. S.; Moore, J. S.; Rodrîguez-Lopez, J.; Sanford, M. S. *J. Am. Chem. Soc*. **2015**, *137*, 14465.
42. Laviron, E. *J. Electroanal. Chem.* **1979**, *101*, 19.

Table of Contents Artwork:

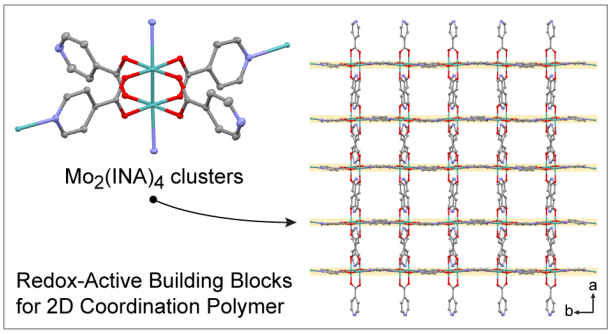

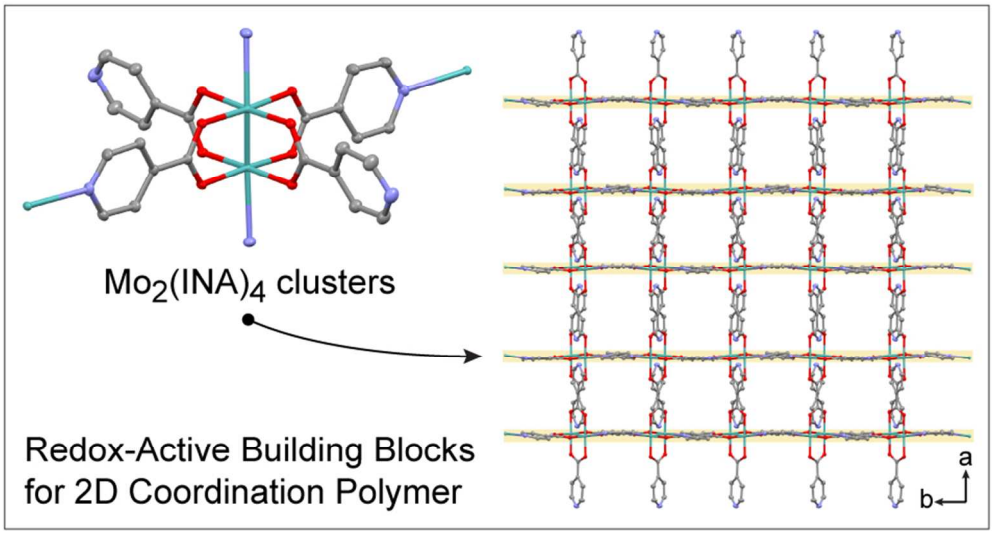

Redox-Active Building Block for 2D Coordination Polymer

81x44mm (300 x 300 DPI)